J Mater Sci (2006) 41:6077–6080
DOI 10.1007/s10853-006-0680-9

LETTER

Cyclic indentation of an elastic-perfectly plastic material

Fuqian Yang · Aditi Saran

Received: 6 March 2006 / Accepted: 17 July 2006 / Published online: 12 August 2006

Fundamental knowledge of the indentation deformation of materials is critical to evaluating dynamic behavior of materials in using the indentation technique. Early studies on the contact of materials provided analytical treatments for both elastic [1–6] and plastic response [7] subjected to dynamic loading. Despite valuable insight into the indentation deformation of materials from analytical approaches, it is difficult to apply these methods in the analysis of the indentation of elastoplastic materials. Consequently, numerical techniques [8–10] were advanced to account for complicated geometries and to establish realistic models. The review of literature indicates that the majority of analytical and numerical solutions of various indentation problems involving elastic and elastoplastic materials have focused on the contact deformation under quasi-static conditions. The obtained solutions might not be applicable to dynamic indentation problems. This has imposed a challenge for using the technique of continuous stiffness measurement to characterize dynamic deformation of thin films and nanoscale structures, which bases on atomic force microscopy and nanoindentation.

The purpose of this work is to use finite element to simulate the dynamic indentation of an elastic-perfectly plastic material by a rigid cylindrical indenter of flat-end. The simulation results will shed a light on understanding dynamic indentation problems as encountered in most nanoindentation tests. In the simulation, we assume: (1) the material is isotropic and homogeneous, (2) the system is isothermal, and (3) the material is not subjected to body force.

For an elastic-perfectly plastic material, the 1-D stress-strain relation subjected to uniaxial stress is

$$\sigma = \begin{cases} E\varepsilon \\ \sigma_y \end{cases} \text{for} \begin{matrix} \varepsilon \le \sigma_y/E \\ \varepsilon \ge \sigma_y/E \end{matrix} \tag{1}$$

where E, ϵ, σ and σ_y are Young's modulus, strain, stress and yield stress, respectively. The corresponding constitutive relation in three dimensions can be established using the von Mises flow rule [11] with no strain-hardening. The linear kinematic relations are used between the components of the strain tensor and the increments of the displacement field.

The simulations are performed with the finite element code ABAQUS [12]. Because of the axial-symmetry of the problem, an axisymmetric finite element model is used. The finite element mesh consists of 6512 nodes, 2075 eight noded axisymmetric quadrilateral elements and 50 five noded axisymmetric infinite elements. To take care of high stress concentration at the edge of the contact zone, refinement of the finite element mesh is accomplished at the contact interface. Coarser meshes are used away from the contact zone. As discussed by Yang and Li [9] in the simulation of the indentation of an Eyring hyperbolic sine material, the round edge of the indenter r / $2a$ (r is the radius of the round edge, and a is the radius of the indenter) in the range of 0.002–0.01 has no effect on the indentation behavior. Thus, r / $2a$ of 0.0025 is used here.

To examine the applicability of the finite element mesh, simulation is first performed for the static indentation of silicon (E = 127 GPa, $v = 0.278$ and

F. Yang (✉) · A. Saran
Department of Chemical and Materials Engineering, University of Kentucky, 177 Anderson Hall, Lexington, KY 40506, USA
e-mail: fyang0@engr.uky.edu

$\sigma_y = 4410$ MPa [13]) by a conical indenter of the included angle 136°. The calculated loading–unloading curves are the same as those given by Bhattacharya and Nix [13], suggesting that the finite element mesh is good enough for the simulation of elastoplastic indentation.

The same finite element mesh is then used in simulating the deformation of an elastic-perfectly plastic material by a cyclic indentation. The material is aluminum, whose mechanical properties are $E = 72$ GPa, $v = 0.3$ and $\sigma_y = 56$ MPa. The radius of the cylindrical, flat-ended indenter is 0.5 μm, and the frequency of the cyclic loading (f) is 9.55 Hz. The median indentation load, F_{med}, varies from 0.55 to 1.22 in the unit of $\pi a^2 \sigma_y$, and the amplitude of the indentation load, ΔF, from 0.45 to 0.8 in the unit of $\pi a^2 \sigma_y$ (note: it requests $|\Delta F| < F_{\text{med}}$ in the simulation). Figure 1 shows a typical indentation load applied to the indenter, which causes the dynamic deformation in the material. In the simulation, the contact between the indenter and the material is assumed to be frictionless.

Figure 2 shows the typical indentation curve for $F_{\text{med}} = 0.045$ mN and $\Delta F = 0.035$ mN. Under the cyclic loading, the indenter continuously moves into the material, which is different from the static indentation of elastic-perfectly plastic materials. This is likely due to the effect of dynamic loading, which causes the dissipation of energy through the propagation of plastic zone underneath the indentation and the propagation of elastoplastic wave. Cyclic indentation can produce a penetration rate (per cycle) as shown in Fig. 2 for small indentation depth. This is in agreement with the observation by Chu and Li [14] in the study of the impression fatigue of β-tin. From Fig. 2, it is found that the indentation depth as a function of the number of cycles, n, can be expressed as

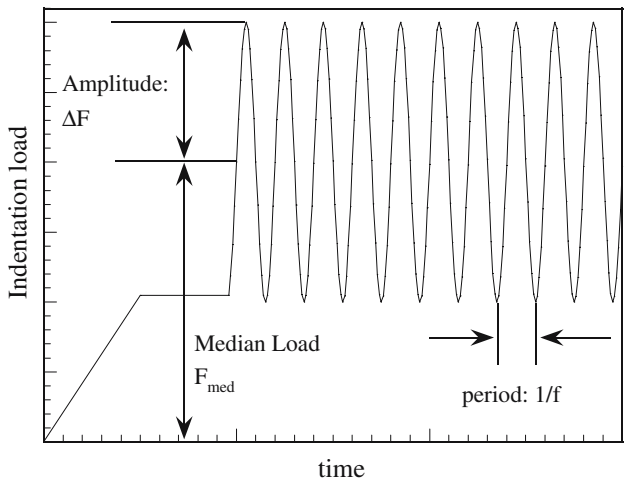

Fig. 1 Schematic of a cyclic indentation load

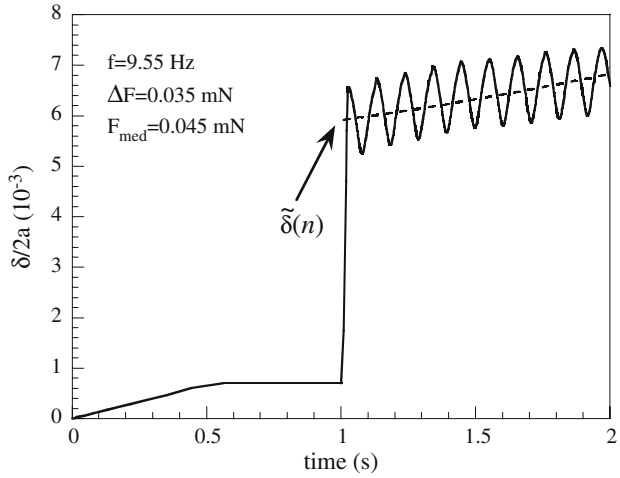

Fig. 2 Time dependence of the indentation depth under a cyclic indentation load

$$\delta(n) = \delta_0 + \tilde{\delta}(n) + \Delta\delta \sin(2\pi n) \tag{2}$$

where δ_0 is the static indentation depth due to the median indentation load, $\tilde{\delta}(n)$ the change of the average indentation depth in each indentation cycle, and $\Delta\delta$ the amplitude of the cyclic indentation depth ($\Delta\delta$ is independent of the number of cycles and can be easily determined). Using Eq. 2 to fit the indentation curves, one can determine the dependence of $\tilde{\delta}(n)$ on the number of indentation cycles, from which one can calculate the average penetration rate ($d\tilde{\delta}/dn$) over the period of the cyclic indentation.

Since the von Mises stress, σ_{eff}, determines the onset and evolution of plastic deformation, the distribution of the von Mises stress is shown in Fig. 3 along the z-axis at both the maximum indentation load and the

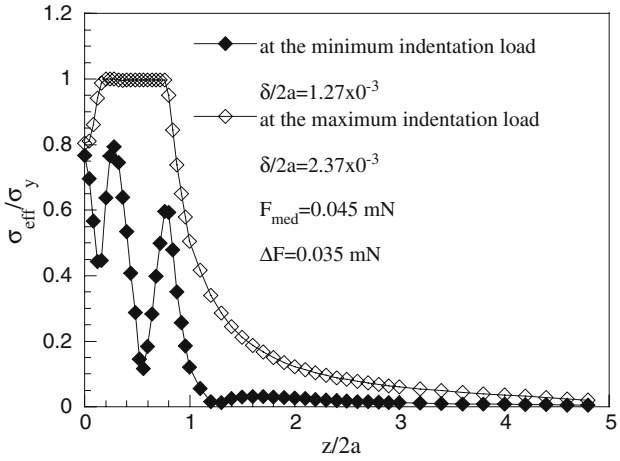

Fig. 3 Distribution of the von Mises stress along the z axis for a cyclic indentation load of $f = 9.55$Hz, $F_{\text{med}} = 0.045$ mN and $\Delta F = 0.035$ mN

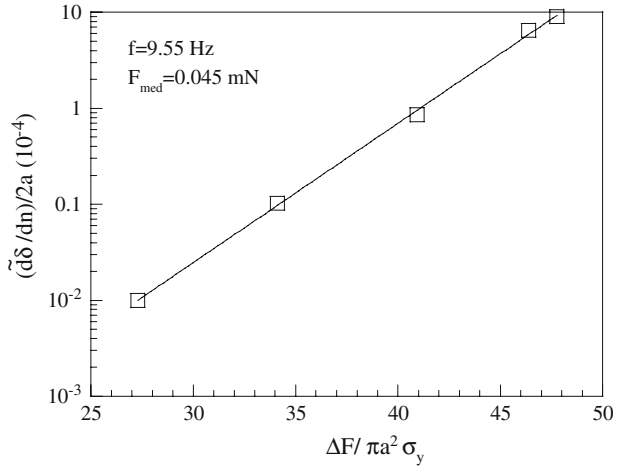

Fig. 4 Dependence of the average penetration rate on the amplitude of the cyclic indentation load

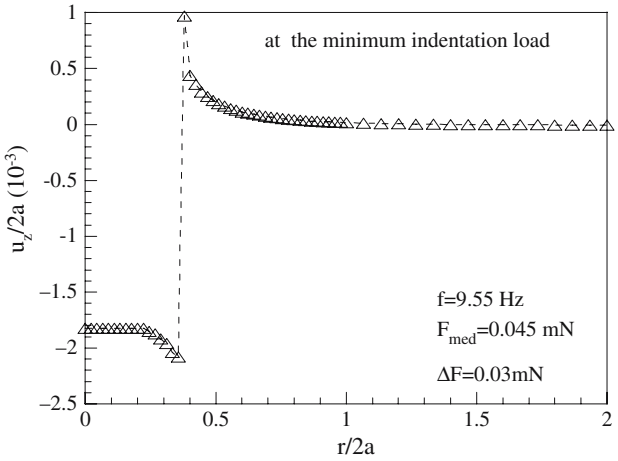

Fig. 6 Surface profile of an indentation at the minimum indentation load

minimum indentation load. At the maximum indentation load, a plastic zone at which $\sigma_{\text{eff}} = \sigma_y$ is observed. The von Mises stress along the z-axis increases with the increase of the distance away from the contact interface, then reaches the value of the yield stress. With the further increase in the distance, it starts to decrease and approaches zero eventually. At the minimum indentation load, the von Mises stress oscillates along the z-axis, which is different from that at the maximum indentation load.

Based on the indentation curves and Eq. 2, the average penetration rate ($d\tilde{\delta}/dn$) at small indentation depth as a function of the cyclic indentation load is evaluated. Figure 4 shows the effect of the amplitude of the cyclic indentation load on the average penetration rate under the same median of the indentation load. For the same median of the indentation load, the

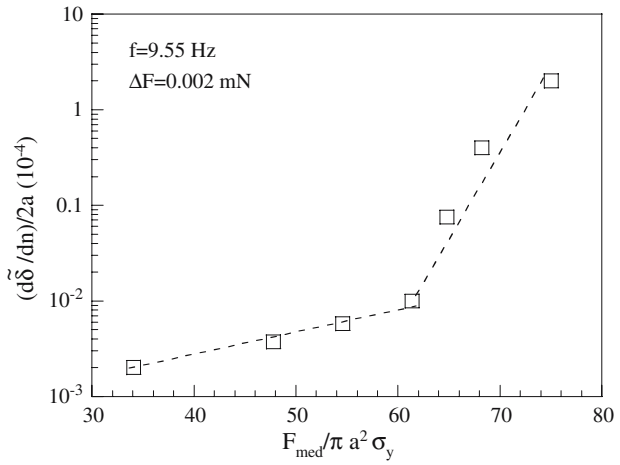

Fig. 5 Dependence of the average penetration rate on the median of the cyclic indentation load

average penetration rate increases with the increase in the amplitude of the cyclic indentation load. Large amplitude will cause the indenter to move deep into the material. The propagation rate of the plastic zone underneath the indentation increases with the increase of the amplitude in the indentation load.

The effect of the median of the indentation load on the average penetration rate under the same amplitude of the cyclic indentation load is shown in Fig. 5. The average penetration rate increases with the increase of the median of the cyclic indentation load. For the ratio of the median of the indentation stress ($F_{\text{med}}/\pi a^2$) to the yield stress being less than 1, the propagation rate of the plastic zone is much smaller than that for the ratio being greater than 1. This is likely due to the formation of relatively larger plastic zone underneath the indentation for the ratio larger than 1, which allows the indenter to move deeper into the material.

The shape of the deformed surface at the minimum indentation load is plotted in Fig. 6. There is upward displacement on the free surface around the indentation, suggesting the formation of pile-up. Local elastic recovery underneath the indentation is observed, at which a small extrusion is formed. The flat-end of the indenter is not in full contact with the material—the contact area changes during the unloading.

On the basis of the simulation results and discussion, the following conclusions can be drawn.

(1) Under cyclic indentation, the plastic zone underneath the indentation propagates into elastic-perfectly plastic materials for small indentation depth.
(2) The average penetration rate of the indenter increases with the increase in the amplitude of the

cyclic indentation load and the median of the indentation load.

(3) The propagation rate of the plastic zone increases with the increase of the amplitude and the median in the indentation load.

Acknowledgement This work is supported by NSF through a grant CMS-0508989, supported by Kentucky Science and Engineering Foundation through a grant KSEF-148–502-03-73, and partially supported by General Motors Corporation.

References

1. Pekeris CL (1955) Proc Natl Acad Sci USA 41:469
2. Lamb H (1904) Phil Trans Royal Soc A203:1
3. Miller GF, Pursey H (1954) Proc Royal Soc A223:521
4. Arnold RN, Bycroft CN, Warburton GB (1955) Trans ASME J Appl Mech 22:391
5. Robertson IA (1966) Proc Cambridge Phil Soc 62:547
6. Gladwell GML (1968) J Sound Vibr 8:215
7. Tirupataiah Y, Sundararajan G (1991) J Mech Phys Solids 39:243
8. Lu J, Suresh S, Ravichandran G (2003) J Mech Phys Solids 51:1923
9. Yang FQ, Li JCM, Shih CW (1995) Mater Sci Eng A 201:50
10. Yang FQ (1998) Int J Mech Sci 40:87
11. Chakrabarty J (2006) Theory of Plasticity. 3rd edn. Butterworth-Heinemann, New York
12. ABAQUS users manual version 5.3, Hibbitt, Karlsson, Sorensen, Inc., Providence, Rhode Island, USA (1994)
13. Bhattacharya AK, Nix WD (1988) Inter J Solids Struc 24:881
14. Li JCM, Chu SNG (1979) Script Metall 13:1021